TELKOMNIKA Indonesian Journal of Electrical Engineering
Vol.12, No.3, March 2014, pp. 2171 ~ 2179
DOI: http://dx.doi.org/10.11591/telkomnika.v12i3.4430

A Nonlinear Numerical Simulation Method of Bionic-Robot-Fish Quick Start

Chao Yang*, Lingyan Sun
School of Materials Engineering, Jiangsu University of Technology
Changzhou, Jiangsu 213001 China, Ph./Fax: +086-86952512/86953281
*Corresponding author, e-mail: yc@jstu.edu.cn

Abstract

Fishtail skeleton, muscles and nerves controlling body swinging were simulated using alloy sheet, giant magnetostrictive material (GMM) posted on this sheet and outside magnetic field in this study. Thus, the quick start of part natural fishes was simulated. The non-linear model related to large geometric deformation and non-linear damping was established after analysis and research. A recurrence formula is obtained using eigensolution, nonlinear dynamic equation and small parameter expansion method, and a numerical method for solving nonlinear problem is formed. The numerical analysis reveals the swimming mechanism of bionic robot fish, and the best start mode of this fish was designed. It also reveals the effect of material, geometric parameters, environmental factors, etc. on the starting of robot fish. The results show that there is an optimum frequency in the starting process of bionic robot fish. The optimum mode is a rapid transition from low order mode to high order mode, thus achieving the quick start of robot fish. These provide a theoretical basis and data support for designing the quick start of bionic robot fish.

Keywords: *bionic robot fish, GMM, magnetic field, quick start, cantilever interlayer sheet*

1. Introduction

Bionic robot can be divided into two categories: general type of robot and micro robot according to the size. The former needs to bring power system, while the latter can rely on vitro system to control. Miniature robot [1] technology has increasingly become the focus of researchers, including super magnetic robot fish [2-5], which has an important research value and broad application prospect. For example, it can safely enter the human body and will not adversely affect various organs in the medical field. It can also be used to work in the place with toxic substances or in contaminated duct and so on in industrial applications.

first bends in C or S shape and then quickly bounces in the starting process to make the body present wavy line. Predatory fish more uses S-shaped starting, and herbivorous fish generally escapes through C-shaped starting. However, the current study on bionic robot fish focuses on the high efficiency features of parade. The studies on the mechanical propulsion mechanism of fish fast start [6] and its project application are very little. Therefore, the study on robot fish with a superior starting performance is very important to improve the high starting efficiency of robot fish. It can provide a theoretical basis and design ideas for the study on robotic fish with a high maneuverability.

2. The Drive Control Equation of Robot Fish

2.1. The Structure Model of Fishtail

Super magnetic robot fish is composed of fish body and fishtail, and the fishtail consists of rectangular alloy sheet of pasted or plated GMM. Cartesian coordinate system was used, and the length, width and height of rectangular fishtail were L, b and h, respectively. Moreover, the pasted or plated thickness $\xi(x)$ of GMM (uniform in the plate width direction) is thinner than alloy sheet: $\xi(x) << h$. The stretching of GMM has a certain relationship with the parameters of outside magnetic field by reference to Clark's (1980) research achievements [7]. The constitutive relation can be expressed as:

$$\varepsilon = \varepsilon_\sigma + \varepsilon_H = S^H \sigma + dH \quad (1)$$

Received August 17, 2013; Revised October 7, 2013; Accepted October 14, 2013

Where, ε represents the total strain, S^H is the compliant coefficient, σ is stress, d is dynamic magnetostrictive coefficient, H is the strength of outside magnetic field. Strain ε_H caused by the outside magnetic field is:

$$\varepsilon_H = \frac{\Delta L}{L} = \lambda = dH \tag{2}$$

λ represents the magnetostrictive coefficient. The strength of outside magnetic field is linearly proportional to the B. Assume that B changes in an exponential relationship:

$$H = B / \mu = B\cos(\Omega t) = B_0(1 + e^{-\varepsilon t})\cos(\Omega t) \tag{3}$$

μ is permeability. The expansion phenomenon of GMM plated on the elastic sheet occurs under the change action of outside magnetic field. Its effects on the sheet can be ultimately transferred into a bending moment distribution:

$$G(x,t) = \int_A \sigma y dA = \int_{h/2}^{\xi(x)+h/2} E_2 dbB_0(1 + e^{-\varepsilon t})\cos(\Omega t) y dy \tag{4}$$

Where $\xi(x) = \xi_0(1 - x/L)$, and ξ_0 is a constant. Moment distribution can be expressed as a quadratic function of the coordinate x:

$$G(x,t) = \xi_0 E_2 dbB_0(1 + e^{-\varepsilon t})(1 - x/L)(\xi_0 - \xi_0 x/L + h)[\cos(\Omega t)]/2$$

2.2. The Nonlinear Mechanics Model of Fishtail Swing

The effect of the GMM layer ($\xi(x) << h$) on the bending rigidity of this structure was ignored to reveal the main mechanical behavior. Then, the problem is reduced to a cantilever beam model. Assume that the fishtail has no torsional deformation in the process of simplifying mechanical model. The fluid resistance to fish-tail swing is approximately equal to its resistance generated in the flow field [8, 9]. The resistance generated on micro-unit is $F_d(x,t) = CV_\infty dx$ when the Reynolds number is low, and the fishtail swings according to the resistance $F_d(LowR_\varepsilon) = (Cons\tan t)\mu V_\infty(Length)$ given by Gerhart [10]. $V_\infty = \partial y(x,t)/\partial t$ in it, and the damping coefficient [10] can be approximated as $C = \mu_0 \pi^2 L/2[\ln(2L/b) - 0.5 + \ln 2]$ where μ_0 is the viscosity coefficient of liquid.

The linear mechanics model of fish-tail swing is [11]:

$$EI\frac{\partial^4 y(x,t)}{\partial x^4} + \rho bh\frac{\partial^2 y(x,t)}{\partial t^2} + C\frac{\partial y(x,t)}{\partial t} = \eta(t) \tag{5}$$

The nonlinear control equation can be established because of taking into account the problems of nonlinear damping and large geometric deformation situation as follow:

$$EI\frac{\partial^4 y(x,t)}{\partial x^4} + \rho bh\frac{\partial^2 y(x,t)}{\partial t^2} + C_1\frac{\partial y(x,t)}{\partial t} + C_2\frac{\partial y(x,t)}{\partial t}\left|\frac{\partial y(x,t)}{\partial t}\right| - \frac{3EA}{2}\left(\frac{\partial y(x,t)}{\partial x}\right)^2\frac{\partial^2 y(x,t)}{\partial x^2} = \eta(x,t) \tag{6}$$

Where, ρ is the density of alloy material, and moment of inertia: $I = bh^3/12$. C1 is the coefficient of linear damping. C2 is the coefficient of nonlinear damping $\eta(t) = \gamma(1 + e^{-\varepsilon t})\cos(\Omega t)$ and $\gamma = -E_2 bdB_0(1 + e^{-\varepsilon t})(\xi_0/L)^2$. The boundary conditions corresponding to the model are:

$$\begin{cases} y(x,t)\ |_{x=0} = 0; \quad \dfrac{\partial y(x,t)}{\partial x}\ |_{x=0} = 0 \\ \dfrac{\partial^2 y(x,t)}{\partial x^2}\ |_{x=L} = 0; \quad \dfrac{\partial^3 y(x,t)}{\partial x^3}\ |_{x=L} = 0. \end{cases} \tag{7}$$

Initial conditions are: $y(x,0)=y_0;\ \ \dot{y}(x,0)=\dot{y}_0(x)=0$ (8)

3. The Method for Solving Control Equations

3.1. Eigenvector Method

The particular solution and general solution of linear Equation (6) were recorded as the following two formulas [12], respectively:

$$y_p=\sum_{n=1}^{\infty}\phi_n^*(t)Y_n(x) \tag{9}$$

$$y_c=\sum_{n=1}^{\infty}\phi_n(t)Y_n(x) \tag{10}$$

The solution of nonlinear problem solution is ordered to be:

$$y=y_c+y_p+y_f=\sum_{n=1}^{\infty}\phi_n(t)Y_n(x)+\sum_{n=1}^{\infty}\phi_n^*(t)Y_n(x)+\sum_{n=1}^{\infty}\bar{\phi}_n(t)Y_n(x) \tag{11}$$

Where, y_f reflects the non-linear nature. If $\bar{\phi}_n(t)$ satisfies $\bar{\phi}_n(t)\big|_{t=0}=\partial\bar{\phi}_n(t)/\partial t\big|_{t=0}=0$, then the Expressions (9) and (10) satisfy initial and boundary conditions. If the Expression (11) satisfies the non-linear Equation (6), then this expression is the solution of the problem. The Expression (11) is substituted into linear Equations (6) to obtain:

$$\begin{aligned}&EI\partial_x^4y_f+\rho bh\partial_t^2y_f+C_1\partial_ty_f+C_2(\partial_ty_c+\partial_ty_p+\partial_ty_f)\left|\partial_ty_c+\partial_ty_p+\partial_ty_f\right|\\&\quad-\frac{3EA}{2}(\partial_xy_c+\partial_xy_p+\partial_xy_f)^2(\partial_x^2y_c+\partial_x^2y_p+\partial_x^2y_f)=0\end{aligned} \tag{12}$$

It can be seen that if y_f can be obtained from Equation (12), then the solution of problem can be obtained by Expression (11).

3.2. Numerical Methods

The small parameter method is used to commence within neighborhood $(-t_0,t_0)$ at t=0, by the time during a very short beginning time（t<<1）. Then:

$$\begin{cases}y_c=\sum_{n=1}^{\infty}\phi_n(t)Y_n(x)\equiv\sum_{n=1}^{\infty}\sum_{m=1}^{\infty}A_{nm}Y_n(x)t^{m-1}\\y_p=\sum_{n=1}^{\infty}\phi_n^*(t)Y_n(x)\equiv\sum_{n=1}^{\infty}\sum_{m=1}^{\infty}B_{nm}Y_n(x)t^{m-1}\\y_f=\sum_{n=1}^{\infty}\bar{\phi}_n(t)Y_n(x)\equiv\sum_{n=1}^{\infty}\sum_{m=1}^{\infty}C_{nm}Y_n(x)t^{m-1}\end{cases} \tag{13}$$

The Expression (11) is the solution of the problem in this period if C_{nm} can be ascertained because A_{nm} and B_{nm} are known. The Equation (12) is as follows at this time:

$$EI\sum_{n=1}^{\infty}\sum_{m=1}^{\infty} C_{nm}Y_n^{(4)}\,t^{m-1}+\rho bh\sum_{n=1}^{\infty}\sum_{m=1}^{\infty}(m-1)(m-2)C_{nm}Y_n\,t^{m-3}+C_1\sum_{n=1}^{\infty}\sum_{m=1}^{\infty}(m-1)C_{nm}Y_n\,t^{m-2}$$
$$+C_2[\sum_{n=1}^{\infty}\sum_{m=1}^{\infty}(m-1)A_{nm}Y_n\,t^{m-2}+\sum_{n=1}^{\infty}\sum_{m=1}^{\infty}(m-1)B_{nm}Y_n\,t^{m-2}+\sum_{n=1}^{\infty}\sum_{m=1}^{\infty}(m-1)C_{nm}Y_n\,t^{m-2}] \quad (14)$$
$$\left|\sum_{n=1}^{\infty}\sum_{m=1}^{\infty}(m-1)A_{nm}Y_n\,t^{m-2}+\sum_{n=1}^{\infty}\sum_{m=1}^{\infty}(m-1)B_{nm}Y_n\,t^{m-2}+\sum_{n=1}^{\infty}\sum_{m=1}^{\infty}(m-1)C_{nm}Y_n\,t^{m-2}\right|$$
$$-\frac{3EA}{2}(\sum_{n=1}^{\infty}\sum_{m=1}^{\infty}A_{nm}Y_n'\,t^{m-1}+\sum_{n=1}^{\infty}\sum_{m=1}^{\infty}B_{nm}Y_n'\,t^{m-1}+\sum_{n=1}^{\infty}\sum_{m=1}^{\infty}C_{nm}Y_n'\,t^{m-1})^2$$
$$(\sum_{n=1}^{\infty}\sum_{m=1}^{\infty}A_{nm}Y_n''\,t^{m-1}+\sum_{n=1}^{\infty}\sum_{m=1}^{\infty}B_{nm}Y_n''\,t^{m-1}+\sum_{n=1}^{\infty}\sum_{m=1}^{\infty}C_{nm}Y_n''\,t^{m-1})=0$$

$$EI\sum_{n=1}^{\infty}\sum_{m=1}^{\infty} C_{nm}Y_n^{(4)}\,t^{m-1}+\rho bh\sum_{n=1}^{\infty}\sum_{m=1}^{\infty}(m+1)mC_{nm+2}Y_n\,t^{m-1}+C_1\sum_{n=1}^{\infty}\sum_{m=1}^{\infty}mC_{nm+1}Y_n\,t^{m-1} \quad (15)$$
$$+C_2\sum_{n=1}^{\infty}\sum_{m=1}^{\infty} D_{nm}Y_n\,t^{m-1}-\frac{3EA}{2}\sum_{n=1}^{\infty}\sum_{m=1}^{\infty} F_{nm}Y_n\,t^{m-1}=0$$

$$\sum_{n=1}^{\infty}\sum_{m=1}^{\infty}F_{nm}Y_n\,t^{m-1}\equiv[\sum_{n=1}^{\infty}\sum_{m=1}^{\infty}(A_{nm}+B_{nm}+C_{nm})Y_n'\,t^{m-1}]^2[\sum_{n=1}^{\infty}\sum_{m=1}^{\infty}(A_{nm}+B_{nm}+C_{nm})Y_n''\,t^{m-1}] \quad (16)$$

$$\sum_{n=1}^{\infty}\sum_{m=1}^{\infty}D_{nm}Y_n\,t^{m-1}\equiv\varsigma(x,t)[\sum_{n=1}^{\infty}\sum_{m=1}^{\infty}m(A_{nm+1}+B_{nm+1}+C_{nm+1})Y_n\,t^{m-1}]^2 \quad (17)$$

Where, $\varsigma(x,t)\equiv\dot{y}/|\dot{y}|$ and $\dot{y}=\sum_{n=1}^{\infty}\sum_{m=1}^{\infty}m(A_{nm+1}+B_{nm+1}+C_{nm+1})Y_n\,t^{m-1}$. The coefficient Equation (15) is compared to obtain:

$$EI\sum_{n=1}^{\infty}C_{nm}Y_n^{(4)}+\rho bh\sum_{n=1}^{\infty}(m+1)mC_{nm+2}Y_n+C_1\sum_{n=1}^{\infty}mC_{nm+1}Y_n+C_2\sum_{n=1}^{\infty}D_{nm}Y_n-\frac{3EA}{2}\sum_{n=1}^{\infty}F_{nm}Y_n=0 \quad (18)$$

Equation (18) is multiplied by $Y_i(x)\quad(i=1,2,\cdots)$, and then the following equation can be obtained by integrating and using orthogonality relationship:

$$C_{nm+2}=\frac{1}{\rho bh(m+1)m}(\frac{3EA}{2}F_{nm}-EIk_n^4C_{nm}-C_1mC_{nm+1}-C_2D_{nm})\quad(n,m=1,2,\cdots) \quad (19)$$

Where, $C_{n1}=C_{n2}=0$, and thus $C_{nm}\quad(m\geq 3)$ can be got through the Equation (19).

The Equations (16) and (17) are multiplied by $Y_i(x)\quad(i=1,2,\cdots)$, respectively. Then, the following equations can be obtained similarly by using the orthogonality relationship and comparison coefficient.

$$F_{nm}=\sum_{n_1=1}^{\infty}\sum_{n_2=1}^{\infty}\sum_{n_3=1}^{\infty}E_{nn_1n_2n_3}\sum_{k=1}^{m}\sum_{j=1}^{k}\gamma_{n_1j}\gamma_{n_2k+1-j}\gamma_{n_3m+1-k}\quad(n,m=1,2,\cdots) \quad (20)$$

$$D_{nm}=\sum_{n_1=1}^{\infty}\sum_{n_2=1}^{\infty}G_{nn_1n_2}\sum_{k=1}^{m}k(m+1-k)\gamma_{n_1k+1}\gamma_{n_2m+2-k}\quad(n,m=1,2,\cdots) \quad (21)$$

Where, $E_{nn_1n_2n_3}\equiv\int_0^l Y_n(x)Y_{n_1}'(x)Y_{n_2}'(x)Y_{n_3}''(x)\,dx$, $G_{nn_1n_2}=\int_0^l\varsigma(x,t)Y_n(x)Y_{n_1}(x)Y_{n_2}\,dx$ and $\gamma_{ij}=A_{ij}+B_{ij}+C_{ij}\quad(i,j=1,2,\ldots)$. and the *N* and *M* may be assigned to *n* and *m*, respectively.

$C_{nk}(k \le m+1)$ is recursively obtained by the former known conditions in discussing $\varsigma(x,t)$ and equation (19), and assume $\dot{y}(x,t,m) = \sum_{n=1}^{N} Y_n [\sum_{k=1}^{M} k(A_{nk+1} + B_{nk+1}) t^{k-1} + \sum_{k=1}^{m+1} (k-1) C_{nk} t^{k-2}]$.

The average driving force can be expressed as:

$$F_{ad} = \frac{1}{\bar{t}} \int_0^{\bar{T}} F(t)dt \equiv \frac{1}{\bar{t}} \int_0^{\bar{T}} \int_0^{l} [C_1 \dot{y}(x,t) + C_2 \dot{y}(x,t) \left| \dot{y}(x,t) \right|] y'(x,t) dx dt \tag{22}$$

Thus, the solution y and the F have been solved in some small neighborhood $(-t_0, t_0)$ at t=0. Then, the solution was sequentially solved in some tiny neighborhood $(-t_0, t_0)$ at $t = t_0$. Therefore, Equation (6) can be written as:

$$EI \frac{\partial^4 y(x,s,t_0)}{\partial x^4} + \rho bh \frac{\partial^2 y(x,s,t_0)}{\partial s^2} + C_1 \frac{\partial y(x,s,t_0)}{\partial s} + C_2 \frac{\partial y(x,s,t_0)}{\partial s} \left| \frac{\partial y(x,s,t_0)}{\partial s} \right| \tag{23}$$
$$- \frac{3EA}{2} (\frac{\partial y(x,s,t_0)}{\partial x})^2 \frac{\partial^2 y(x,s,t_0)}{\partial x^2} = \eta(x,s,t_0)$$

The initial condition is $y\big|_{t=t_0} \equiv y\big|_{s=0} = \tilde{y}_0(x,t_0),\ \dot{y}\big|_{t=t_0} \equiv \dot{y}\big|_{s=0} = \dot{\tilde{y}}_0(x,t_0)$ at this time,

$$\begin{cases} \tilde{y}_0(x,t_0) = \sum_{n=1}^{N} (A_{n1} + B_{n1} + C_{n1}) Y_n(x) \\ \dot{\tilde{y}}_0(x,t_0) = \sum_{n=1}^{N} (A_{n2} + B_{n2} + C_{n2}) Y_n(x) \end{cases} \tag{24}$$

They are substituted into the linear Equation (5) to get:

$$\begin{cases} \sum_{i=1}^{\infty} \phi_i(0) Y_i(x) + \sum_{i=1}^{\infty} \phi_i^*(0) Y_i(x)) dx = \tilde{y}_0(x,t_0) \\ \sum_{i=1}^{\infty} \dot{\phi}_i(t) Y_i(x) + \sum_{i=1}^{\infty} \dot{\phi}_i^*(t) Y_i(x) = \dot{\tilde{y}}_0(x,t_0) \end{cases} \tag{25}$$

The both sides of above Equation (25) were multiplied by Yj(x) at the same time and then integrated along the beam. Then, equations were got by using orthogonality relationship between mode shape functions:

$$\begin{cases} \int_0^l Y_i^2(x)dx \sum_{i=1}^{\infty} (\phi_i(0) + \phi_i^*(0)) = \int_0^l \tilde{y}_0 Y_j(x)dx \\ \int_0^l Y_i^2(x)dx \sum_{i=1}^{\infty} (\dot{\phi}_i(t) + \dot{\phi}_i^*(t)) = \int_0^l \dot{\tilde{y}}_0 Y_j(x)dx \end{cases} \tag{26}$$

$$\begin{cases} \phi_i(0) + \phi_i^*(0) = \frac{\tilde{z}_i}{B_i} \\ \dot{\phi}_i(t) + \dot{\phi}_i^*(t) = \frac{\tilde{g}_i}{B_i} \end{cases} \tag{27}$$

Where, $\tilde{z}_i = \int_0^l \tilde{y}_0 Y_j(x)dx$, $\tilde{g}_i = \int_0^l \dot{\tilde{y}}_0 Y_j(x)dx$. Thus, the unknown coefficients c_1 and c_2 can be obtained:

$$\begin{cases} c_{1i} = \frac{\frac{\tilde{z}_i}{B_i} r_2 - a_i r_2 - \frac{\tilde{g}_i}{B_i} + b_i \Omega}{r_2 - r_1} \\ c_{2i} = \frac{\frac{\tilde{z}_i}{B_i} r_1 - a_i r_1 - \frac{\tilde{g}_i}{B_i} + b_i \Omega}{r_1 - r_2} \end{cases} \quad \Delta_i > 0 \qquad \begin{cases} c_{1i} = \frac{\tilde{z}_i}{B_i} - a_i \\ c_{2i} = \frac{\tilde{g}_i}{B_i} - b_i \Omega - \alpha \left(\frac{\tilde{z}_i}{B_i} - a_i \right) \end{cases} \quad \Delta_i = 0 \qquad \begin{cases} c_{1i} = \frac{\tilde{z}_i}{B_i} - a_i \\ c_{2i} = \frac{\frac{\tilde{g}_i}{B_i} - b_i \Omega - \alpha \left(\frac{\tilde{z}_i}{B_i} - a_i \right)}{\beta_i} \end{cases} \quad \Delta_i < 0$$

Then, the general solution y_c has been solved. The particular solution and general solution of similar linear Equation (5) are recorded as:

$$y_p = \sum_{n=1}^{\infty} \phi_n^*(t_0 + s) Y_n(x) \tag{28}$$

$$y_c = \sum_{n=1}^{\infty} \phi_n(t_0 + s) Y_n(x) g \tag{29}$$

It can be verified that $y_c + y_p$ satisfies the linear Equation (5) and the initial and boundary conditions.

The case $(t = t_0)$ was studied at any time in the following study. $s = t - t_0$ was ordered, and $|t - t_0|$ □ 1 or $|s|$ □ 1, thus the following equation can be obtained by expanding by s:

$$\begin{cases} y_c = \sum_{n=1}^{\infty} \phi_n(t_0 + s) Y_n(x) \equiv \sum_{n=1}^{\infty} \sum_{m=1}^{\infty} A_{nm} Y_n(x) s^{m-1} \\ y_p = \sum_{n=1}^{\infty} \phi_n^*(t_0 + s) Y_n(x) \equiv \sum_{n=1}^{\infty} \sum_{m=1}^{\infty} B_{nm} Y_n(x) s^{m-1} \\ y_f = \sum_{n=1}^{\infty} \bar{\phi}_n(t_0 + s) Y_n(x) \equiv \sum_{n=1}^{\infty} \sum_{m=1}^{\infty} C_{nm} Y_n(x) s^{m-1} \end{cases} \tag{30}$$

Assume that the displacement and velocity distribution at $t = t_0$ are known, A_{nm} and B_{nm} are also known. If C_{nm} can be determined, then Formula (11) is the solution of problem in this period of time. Equation (12) can similarly be simplified to:

$$\begin{aligned} &EI \sum_{n=1}^{\infty} \sum_{m=1}^{\infty} C_{nm} Y_n^{(4)} s^{m-1} + \rho bh \sum_{n=1}^{\infty} \sum_{m=1}^{\infty} (m+1) m C_{nm+2} Y_n s^{m-1} + C_1 \sum_{n=1}^{\infty} \sum_{m=1}^{\infty} m C_{nm+1} Y_n s^{m-1} \\ &+ C_2 \sum_{n=1}^{\infty} \sum_{m=1}^{\infty} D_{nm} Y_n s^{m-1} - \frac{3EA}{2} \sum_{n=1}^{\infty} \sum_{m=1}^{\infty} F_{nm} Y_n s^{m-1} = 0 \end{aligned} \tag{31}$$

$$\sum_{n=1}^{\infty} \sum_{m=1}^{\infty} F_{nm} Y_n s^{m-1} \equiv [\sum_{n=1}^{\infty} \sum_{m=1}^{\infty} (A_{nm} + B_{nm} + C_{nm}) Y_n' s^{m-1}]^2 [\sum_{n=1}^{\infty} \sum_{m=1}^{\infty} (A_{nm} + B_{nm} + C_{nm}) Y_n'' s^{m-1}] \tag{32}$$

$$\sum_{n=1}^{\infty} \sum_{m=1}^{\infty} D_{nm} Y_n s^{m-1} \equiv \varsigma(x,s) [\sum_{n=1}^{\infty} \sum_{m=1}^{\infty} m (A_{nm+1} + B_{nm+1} + C_{nm+1}) Y_n s^{m-1}]^2 \tag{33}$$

Where, $\varsigma(x,t) \equiv \dot{y} / |\dot{y}|$ and $\dot{y} = \sum_{n=1}^{\infty} \sum_{m=1}^{\infty} m (A_{nm+1} + B_{nm+1} + C_{nm+1}) Y_n t^{m-1}$. The coefficient Equation (15) is compared to obtain:

$$EI \sum_{n=1}^{\infty} C_{nm} Y_n^{(4)} + \rho bh \sum_{n=1}^{\infty} (m+1) m C_{nm+2} Y_n + C_1 \sum_{n=1}^{\infty} m C_{nm+1} Y_n + C_2 \sum_{n=1}^{\infty} D_{nm} Y_n - \frac{3EA}{2} \sum_{n=1}^{\infty} F_{nm} Y_n = 0 \quad (m=1,2,..) \tag{34}$$

Equation (18) is multiplied by $Y_i(x)$ $(i = 1, 2, \cdots)$, and then the following equation can be obtained by integrating and using orthogonality relationship:

$$C_{nm+2} = \frac{1}{\rho bh (m+1) m} (\frac{3EA}{2} F_{nm} - EJ k_n^4 C_{nm} - C_1 m C_{nm+1} - C_2 D_{nm}) \quad (n, m = 1, 2, \cdots) \tag{35}$$

Where, $C_{n1} = C_{n2} = 0$ and C_{nm} $(m \geq 3)$ can be got through Equation (35). The Equations (16) and (17) are multiplied by$Y_{i(x)}$, respectively. Then, the following equations can be obtained similarly by using the orthogonality relationship and comparison coefficient:

$$F_{nm} = \sum_{n_1=1}^{\infty}\sum_{n_2=1}^{\infty}\sum_{n_3=1}^{\infty} E_{nn_1n_2n_3}\sum_{k=1}^{m}\sum_{j=1}^{k}\gamma_{n_1j}\gamma_{n_2k+1-j}\gamma_{n_3m+1-k} \quad (n,m=1,2,\cdots) \tag{36}$$

$$D_{nm} = \sum_{n_1=1}^{\infty}\sum_{n_2=1}^{\infty} G_{nn_1n_2}\sum_{k=1}^{m} k(m+1-k)\gamma_{n_1k+1}\gamma_{n_2m+2-k} \quad (n,m=1,2,\cdots) \tag{37}$$

$E_{nn_1n_2n_3} \equiv \int_0^l Y_n(x)Y'_{n_1}(x)Y'_{n_2}(x)Y''_{n_3}(x)\,dx$, $G_{nn_1n_2} = \int_0^l \varsigma(x,t)Y_n(x)Y_{n_1}(x)Y_{n_2}\,dx$ and $\gamma_{ij} = A_{ij} + B_{ij} + C_{ij}$ $(i,j=1,2,\ldots)$ respectively. $C_{nk}(k \leq m+1)$ was known when $\varsigma(x,t)$ and Equation (36) were discussed, and $\dot{y}(x,t,m) = \sum_{n=1}^{N} Y_n\,[\sum_{k=1}^{M} k(A_{nk+1} + B_{nk+1})t^{k-1} + \sum_{k=1}^{m+1}(k-1)C_{nk}t^{k-2}]$ was ordered. Therefore, the mean force can be expressed as:

$$F_{ad} = \frac{1}{\bar{t}}\int_0^{\bar{t}} F(t)dt \equiv \frac{1}{\bar{t}}\int_0^{\bar{t}}\int_0^l [C_1\dot{y}(x,t) + C_2\dot{y}(x,t)\left|\dot{y}(x,t)\right|]y'(x,t)dxdt \tag{38}$$

The small parameter expansion continued in some small neighborhood $\left(-t_0, t_0\right)$ of $t = 2t_0$, and the things like this were done in turn ... Thus, the swing vibration mode y and the average driving force F_{ad} of fishtail can be got under the non-linear model.

3.3. The Swimming Speed of Robot Fish

Suppose that displacements of mass center are u_x and u_y in *x* and *y* directions when robot fish swims forward, respectively, and rotation angle is θ. The driving force is divided into the component forces F_x and F_y in two directions, respectively. Then, the equation of motion can be expressed as Equation (39):

$$\begin{cases} \ddot{u}_x = \int_0^L F_x(x,t)dx \\ \ddot{u}_y + C_r\ddot{u}_y = \int_0^L F_y(x,t)dx \\ J\ddot{\theta} = \int_0^L (F_y(x,t)x - F_x(x,t)y)dx \end{cases} \tag{39}$$

4. Numerical Results and Analysis

The selected parameters are as follows: $\xi_0 = 1.0\times10^{-5}[\mathrm{m}]$, $b = 1.0\times10^{-2}[\mathrm{m}]$, $h = 1.0\times10^{-4}[\mathrm{m}]$. $\mu_0 = 2.0[\mathrm{Pa\cdot s}]$. $E = 7.0\times10^{9}[\mathrm{Pa}]$, $\rho = 2.0\times10^{3}[\mathrm{kg/m^3}]$, the selected GMM [10] is $\mathrm{TbFe_2}$ ($E_2 = 9.4\times10^{10}[\mathrm{Pa}]$, $d = 3.77\times10^{-6}[\mathrm{m/A}]$ and $B_0 = 10[\mathrm{T}]$), and the first five orders of modal superposition is chosen. L=0.09 is selected as the fishtail length [11]. The time required by fishtail swing for three times under the second order frequency is ordered to be start time. Figure 1 shows the relation curve of mean force and the frequency of outside magnetic field. This figure also shows that the curve has a maximum, and the frequency of outside magnetic field at this point is 40. These indicate that there exists an optimal frequency of outside magnetic field, and the average driving force inspired at this frequency is largest.

The swing shape of fishtail is shown in Figure 3 at the optimum frequency of outside magnetic field. This figure shows that fishtail is initially bent into C shape and then transited to

the S shape. The swinging shape of S-shaped fishtail is the gesture of quick start [2-4]. This conclusion explains the quick start mechanism of bionic robot fish.

Figure 2 shows the vibration modes corresponding to the first three orders of natural frequencies to further illustrate the swing shape of fishtail. The comparison between Figure 4(a) and (b) shows that the first-order vibration mode is the major component in the early period of robot fish starting. Then, the second-order natural vibration mode becomes the major component. Figure 4 shows the coefficient change rule of each-order natural vibration mode with time in Solution (14) of variation shape to more clearly show the process. Figure 4(b) clearly shows that the first-order vibration mode coefficient shows an attenuation trend, and the second-order and third-order vibration mode coefficients play a dominant role. Swing shape is mainly changed to the high-order natural vibration mode. This starting can be considered as S-shaped starting.

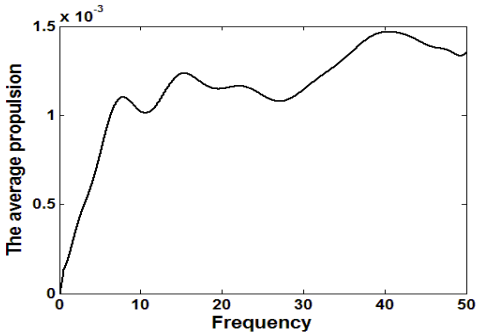

Figure 1. Relationship between External Frequency and Average Driving Fore

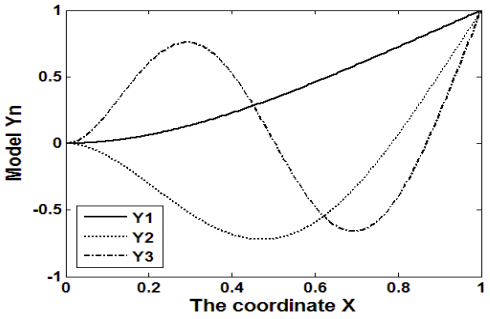

Figure 2. First Three Orders of Vibration Modes

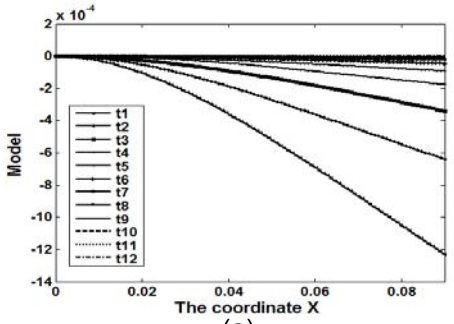

(a)

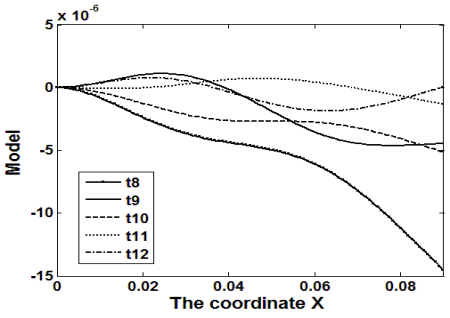

(b)

Figure 3. Swing Vibration Modes of Fishtail under the Excitation of External Magnetic Field

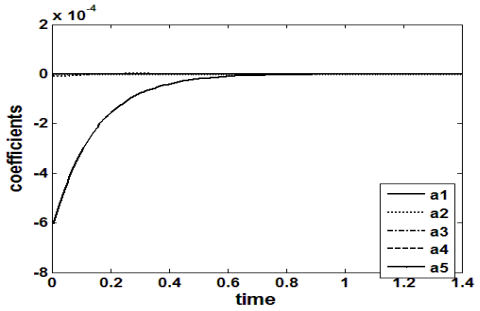

(a)

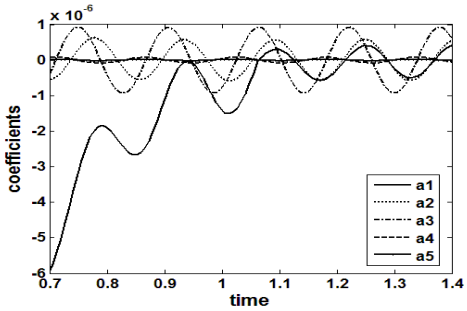

(b)

Figure 4. Coefficients of Vibration Modes

Figure 5 shows the entire starting process of bionic super-magnetic robot fish. It is noted that the starting trajectory of robot fish is along an arc. There is an angle between it and the initial starting of fish body. This is caused by the inconformity between the resultant direction of driving forces and the direction of fish body. The angle is relevant to the strength of outside magnetic field, frequency and other factors: the initial degree of bend and the speed of backswing. Therefore, these factors should be considered in the quick start design of robot fish.

Figure 5. Starting Process of Robot Fish

5. Conclusion

The starting speed of GMM robot fish can be controlled by adjusting the frequency and intensity of the outside magnetic field. How fast GMM robot fish starts is related to geometric parameters, liquid environment, material constants and the frequency and intensity of the outside magnetic field. Fishtail is first bent to C-shape in the starting process of robot fish and then transited to C-shape, S-shape or S+C-shape and so on. The proportion of natural vibration mode in the solution determines the starting form of GMM bionic fish. There is an angle between the trajectory in the starting process of bionic fish and fish body. This angle is closely related to the frequency and intensity of outside magnetic field. The research results verify the rationality of fish S-shaped starting and also provide a theoretical basis for the design of bionic robot fish with quick start.

Acknowledgements

This work was supported by National Natural Science Fund of China (51105181).

References

[1] Otsuka A. *Development of an eating function support system*. Proc.[1]st IARP Workshop Medical and Healthcare Robots, Ottawa, Canada. 1988; 6: 789-792.
[2] Sun FM, Xu XS, et al. Non-linear Vibration and Dynamic Characteristic of Fish-like Robot Controlled by GMM Actuator. *Journal of Intelligent Material Systems and Structures*. 2009; 20: 1503-1513.
[3] Sun FM, Xu XS. The Control Mechanism of a New Fish-Like Underwater Robot with Two Tails. *Lecture Notes in Computer Science*. 2008; LNAI 5314(1): 304-313.
[4] Xu XS, Sun FM, Wang GP. The control and optimization design of the fish-like underwater robot with the aid of the giant magnetostrictive material actuator. *Journal of Vibration and Control.* 2009; 15(10): 1443–1462.
[5] Schriefer JE, Hale ME. Strikes and startles of northern pike (Esox lucius): a comparison of muscle activity and kinematics between S- start behaviors. *J Exp. Biol*. 2004; 207: 535- 544.
[6] Chen Hong, Zhu Changan, Yin Xiezhen, Xing Xiaozheng. Research on fast-start performance of fish-like underwater robot. *Journal of Ship Mechanics*. 2007; 11(5): 647-654.
[7] Clark AE. *Ferromagnetic Material*. Wohlfath EP, North-Holland Publishing Company. 1980.
[8] Ji Hengteng, Fan Ju, Huang Xianglu. Numerical simulation of hydrodynamic forces of heave plate. *Journal of Shanghai Jiaotong University*. 2003; 37 (8): 1266-1270.
[9] Prislin I, Blevins RD, Halkyard JE. *Viscous damping and added mass of so lid square plates*. Proceedings of the International Conference on Offshore Mechanics and Arctic Engineering. ASME Fairfield NJUSA. 1998: 5-9.
[10] Gerhart PM, Gross RJ, Hochstein JI. *Fundamentals of Fluid Mechanics*. 2nd Edition. Addison Wesley. 1992.
[11] Chao Yang. A Numerical Analytical Method of Parameter Optimization for Fast-starting of the Bionic Robot fis. *International Journal of Online Engineering*. 2013; 9(7): 10-14.
[12] Zhang Yahui, Lin Jiahao. *Fundamentals of Structural Dynamics*. Dalian. Dalian University of Technology Press. 2007.